A New Device for High-Speed Biaxial Tissue Testing: Application to Traumatic Rupture of the Aorta

Matthew J. Mason, Chirag S. Shah, Muralikrishna Maddali, King H. Yang, Warren N. Hardy
Wayne State University, Bioengineering Center
Chris A. Van Ee
Design Research Engineering
Kennerly Digges
FHWA/NHTSA National Crash Analysis Center, The George Washington University.

ABSTRACT
A biaxial test device was designed to obtain the material properties of aortic tissue at rates consistent with those seen in automotive impact. Fundamental to the design are four small tissue clamps used to grasp the ends of the tissue sample. The applied load at each clamp is determined using subminiature load cells in conjunction with miniature accelerometers for inertial compensation. Four lightweight carriages serve as mounting points for each clamp. The carriages ride on linear shafts, and are equipped with low-friction bearings. Each carriage is connected to the top of a central drive disk by a rigid link. A fifth carriage, also connected to the drive disk by a rigid link, is attached at the bottom. A pneumatic cylinder attached to the lower carriage initiates rotation of the disk. This produces identical motion of the upper carriages in four directions away from the disk center. Initial slack in a low-stretch, high-strength rope connects the cylinder to the lower carriage and allows the cylinder to achieve the desired test speed before initiating motion in the carriages. Two lasers, focused on the top and bottom surfaces of the tissue samples measure sample thickness throughout a given test.

INTRODUCTION
A number of research efforts have attempted to quantify the mechanical properties of aortic tissue. Considerable work has been done within the physiologic range (Silver, 1989) of stress and strain. Other efforts include pressure-volume tests, bubble inflation tests, and uniaxial and biaxial tensile tests.

Pressure-Volume Testing Methods
Early on, Hallock and Benson (1937) obtained a pressure-volume relationship for human cadaver aortas. Cylindrical specimens were pressurized using saline. The volume of saline in the specimen determined the change in volume. Pressure was applied incrementally. Elasticity was found to decrease with increase in specimen age. Later, Bergel (1961) determined pressure-radius relationships in static experiments on thoracic and abdominal canine aorta, and was the first to suggest incremental modulus for nonlinear stress-strain relationships. The modulus of elasticity varied from 0.12 to 1.81 MPa for internal pressure of 5.3 and 29.3 kPa, respectively. These tests could not examine time dependent aspects of the tissue behavior. Gow and Taylor (1968) conducted *in-vivo* experiments on dogs to estimate the dynamic and viscous moduli, which incorporated the results of Bergel (1961). Calipers sewn to the adventitia of the aorta recorded the diameter of the aorta. Lag between the stress and strain provided a measure of viscosity.

Collins and Hu (1972) tested porcine aorta specimens approximately 125-mm long. Radial expansion was constrained as the specimens were deformed longitudinally. Extension was monitored using a 400-fps camera. A pressure transducer was inserted in a plug at the end of the aorta, which also had an accelerometer mounted to it. Comparison between static and dynamic stress-strain curves indicated the tissue was stiffer at higher strain rates. Circumferential rupture of the aorta occurred at higher stress and lower strain as strain rate increased. The modulus was found to be 0.4 -1.0 MPa for rates up to 3.5 sec^{-1}.

Uniaxial Testing Methods

Lundevall (1964) studied tensile properties of advantitia-free strips of the human aorta in four different regions using dumbbell shaped specimens. Using the strength of the ascending aorta for reference, the strength of the isthmus and the descending aorta were found to have sixty-three percent and eighty percent of baseline strength, respectively. Aortic tissue prepared in this fashion was found to be nonlinear, anisotropic, and rate sensitive.

Within the physiologic range proposed by Fung (1993), Viano (1983) reported that the elastic modulus of the human aorta ranged from 360 to 400 kPa in the circumferential direction and 220 to 300 kPa in the longitudinal direction. Its stiffness increased dramatically when the load exceeded the physiologic range or when the strain rate was increased. Mohan and Melvin (1982) conducted uniaxial tensile tests to determine failure properties of aortic tissue at rates on the order 100 sec^{-1}. Dumbbell-shaped specimens were stamped out of the thoracic aorta of human cadavers, in both longitudinal and transverse directions. A mechanical testing machine was used to precondition and test the specimens. High-speed film (1000 fps) was used to record deformation. The ultimate stress in the transverse direction (5.07 MPa) was found to be 1.54 times that in the longitudinal direction (3.53 MPa) for dynamic loading. The ultimate stress for dynamic loading was 1.87 times the quasi-static value in the longitudinal direction and 1.84 times the quasi-static value in the transverse direction.

Biaxial Testing Methods

Uniaxial tests cannot provide the full relationship between stress and strain for a given sample. Biaxial tests simultaneously load the tissue in different directions and provide a more complete estimate of material properties. A number of biaxial tissue testing issues and phenomena are reviewed by Sacks (2001). Specifically mentioned are the desire to maintain uniform states of stress and strain within the target region of the sample, and the need to keep the target region away from the sample edges to minimize the effects of the attachments to the sample. Free expansion of the sample edges in the lateral direction is also suggested. However, the scale of the measurements versus the continuum assumption for specific tissues can present problems when attempting to relate the mechanical response to the tissue structure. Further, the behavior of tissues at the continuum scale (1 micron) can manifest in complex behavior measured at the macro level. The author states, "Accounting for these behaviors in both experimental evaluation and formulation of appropriate constitutive models continues to be challenging."

Mohan and Melvin (1983) conducted bubble inflation experiments on human cadaver aortas. Circular specimens (6.5 or 5 cm diameter) were cut from the aorta wall. A circular grid was imprinted on each specimen and the axial direction was marked. Quasistatic tests (0.01 s^{-1}) resulting in tissue failure were conducted. A camera recorded deformations of the circular grid

and a pressure transducer measured pressure. Dynamic tests ($20s^{-1}$) were conducted by pressurizing specimens between 690 and 970 kPa. Deformation due to pressure was assumed to be spherical with maximum deformation at the pole. The diameter and radius of curvature for the innermost circle was measured and the extension ratios were determined. The failure pressure, and therefore stress, for dynamic conditions was over two times greater than the failure pressure for quasi-static conditions. Little difference was found between the uniaxial and biaxial ultimate stresses and extension ratios. In these tests, specimens were deformed using a uniform state of stress. The response of tissue loaded along two perpendicular directions cannot be analyzed through pressure inflation techniques. Better understanding of mechanical tissue properties can be obtained through the use of biplane testing techniques.

Nielsen et al. (1991) developed a biaxial testing machine to determine the mechanical properties of highly deformable membrane tissues. Four steel strings connected the specimen to electromechanical vibrators (dc 90 Hz, +/- 2.5 mm). Forces at each point of tethering could be monitored and adjusted. Video cameras were used to collect strain data.

A similar technique was applied by Bass et al. (2001) to the study of porcine aorta for 20 and 65 Hz. Samples were dissected to be 25-mm square with the edges aligned with the longitudinal and circumferential axes of the aorta. Constants were derived from the data to fit an anisotropic hyperelastic material assumption. This study also examined over-pressurization of *in vitro* and *in situ* human aorta specimens. A majority of these tests resulted in longitudinal tears, which are to be expected given the aorta is viewed as a thin-walled cylindrical vessel, but do not reflect injuries seen in the field.

Demer and Yin (1983) conducted biaxial experiments on canine myocardium. Square samples (3cm) were marked with four strips of black carbon paper, which were glued to the center of each specimen in a 1-cm square pattern. Video cameras were used to record deformations. Suture was used to connect the tissue to the pulling apparatus in each of the four directions. The suture was looped around needles that were inserted along each sample edge to better distribute load. This technique was thought to produce less tissue damage, and therefore "stray compliance", than clamping techniques, and less tissue tearing than typical suture techniques, while allowing the specimens freedom of lateral movement. The apparatus was able to produce velocities ranging from 0.025 to 2.5mm/sec.

Sacks and Chuong (1993) conducted experiments on myocardium from 5 mongrel dogs using a biaxial machine with speeds from 0.38 to 22.86 mm/sec. A set of staples and sutures along each side of the square specimens (35mm) was used to attach the samples to the testing device. The specimens were stretched by stepper actuators. To measure tissue deformation, two thin strips of black tape glued to each specimen were tracked by cameras.

Zhou and Fung (1997) examined nonlinearity in the stress strain response for canine aortic tissue. Each side of a square tissue specimen (3 cm) of 0.18 cm thickness was stapled and connected by silk threads to a force transducer. Video dimensional analysis was used to calculate strain. Lagrangian stresses were calculated also.

Boreik et al. (2000) conducted biaxial experiments on canine diaphragms. Square specimens (5cm) were excised from the tissue. Four markers bounding a 1-cm square were placed at the middle of each specimen, and were used to measure tissue deformation. Stepper motors and force transducers were attached to opposite ends of each axis. Ten threaded fishhooks placed at 5mm intervals connected each specimen edge to its corresponding apparatus component.

METHODS

The assembled test device is shown in Figure 1 (top view) and Figure 2 (bottom view). The main components of the device are indicated by arrows and include: main plate (1), rails (2), upper carriages (3), clamps (4), load cells (5), upper links (6), drive disk (7), drive arm (8), lower carriage (9), lower link (10), and main bearing (not visible in the assembled device).

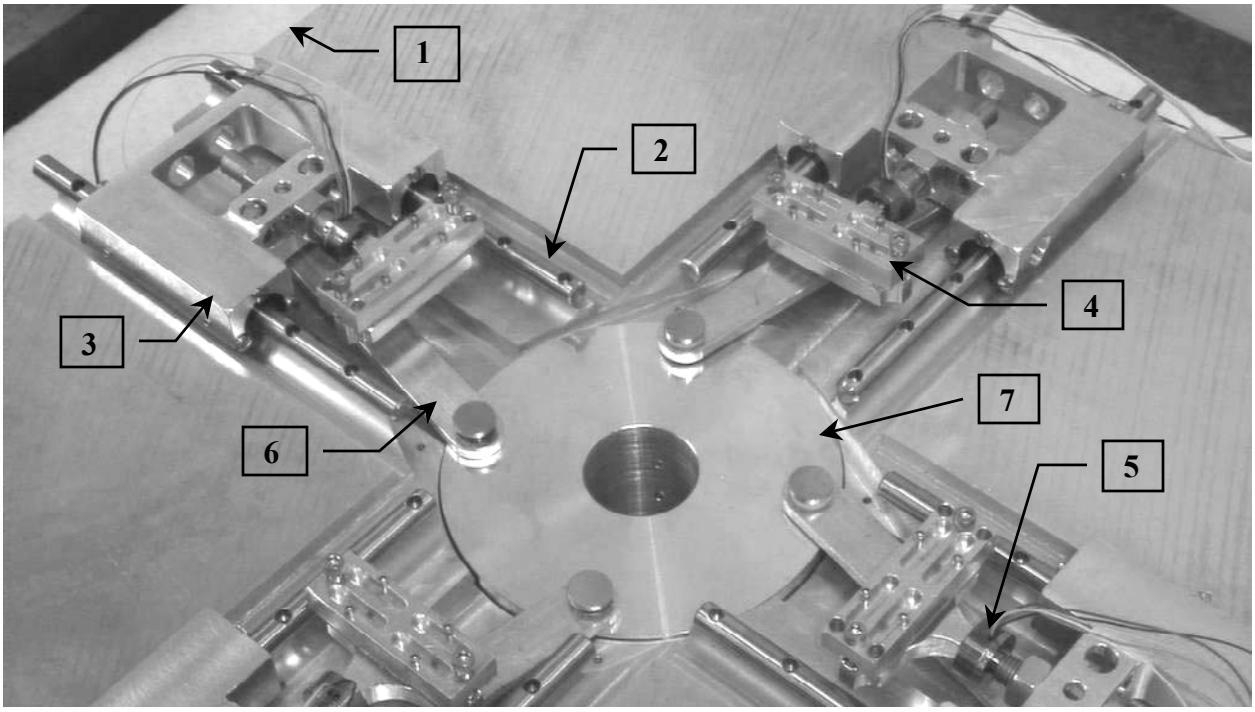

Figure 1: Complete assembly (top view).

A description of the individual components is followed by a section on assembly of the complete test device. The function and design of each component are outlined. Components are machined from billet aluminum (6061-T6 alloy) unless otherwise noted, aluminum being preferred for its strength, light weight, and ease of machining. Stainless steel fasteners are used exclusively. Device materials are selected in all instances for their corrosion resistance to solutions associated with tissue testing. Mechanical drawings of select components are provided in the Appendix.

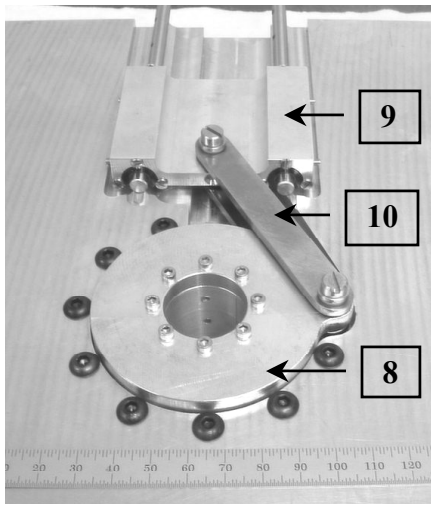

Fig. 2: Complete assembly (bottom view).

Main Plate

The main plate (Fig. 3) serves as a mounting platform and housing for the various assemblies incorporated into the working test device. Precision cast and ground aluminum is used for its consistent thickness and ease of machining. Plate dimensions are 33.0 x 33.0 x 5.1 cm (13.0 x 13.0 x 2.0 inches). Four pairs of stainless steel 6.35-mm (¼ inch) diameter linear shafts are mounted in the plate's top face. The shaft pairs are arranged about a stepped bore machined in the plate center. Shaft pair orientation corresponds to 0°, 90°, 180°, and 270° as designated by standard convention. The shafts run approximately from the bore edge to the plate's outer edge. Each shaft in a pairing is offset 25.4 mm (1.0 inch) from the bore centerline to give a 50.8-mm (2-inch) center-to-center spacing. Machined pockets and channels in the plate top provide clearance for the upper carriages and associated linkage.

A single pair of linear shafts is mounted to the plate bottom. Shaft orientation corresponds to 0°, with the upper 0° shaft pair lying directly underneath. Holes drilled in the bore step receive the main bearing attachment screws.

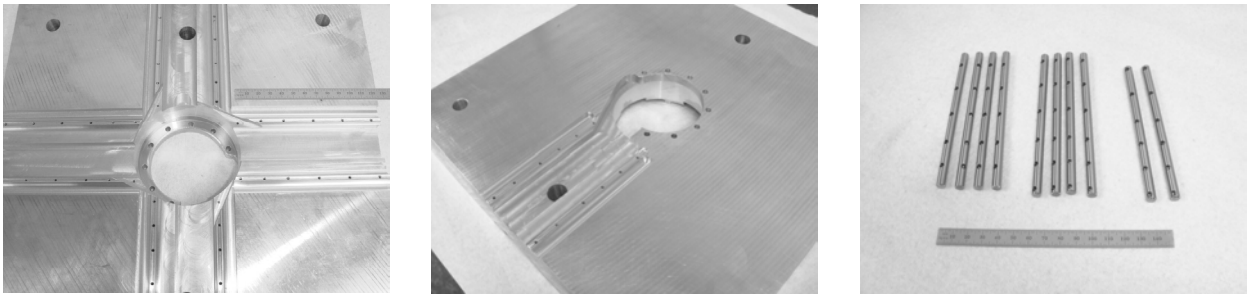

Fig. 3: Main plate and rails. From left to right: plate top, plate bottom, and carriage rails.

Main Bearing

The main bearing is the low-friction surface on which the drive disk turns. The bearing is machined from SAE 841 oil-impregnated sintered bronze and rests in the main plate center bore (Fig. 4). Tapped holes in the bearing's stepped region are used to secure it to the main plate. The bearing bore inner diameter (ID) is machined to the minimum size required for bind-free rotation of the drive disk.

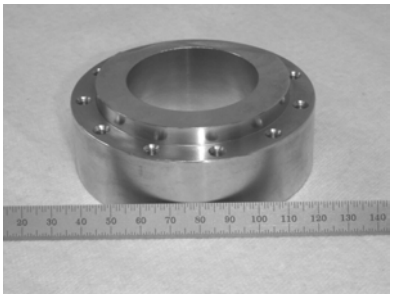

Fig. 4: Main bearing.

Drive Disk

The drive disk transfers the rotary motion imparted to it by the drive arm to the upper carriages via the attached upper links. It is a flanged design incorporating a Teflon® sleeve and lining (Fig. 5). The Teflon® provides a very low friction interface between the disk and the main bearing. A 25.4-mm (1-inch) hole drilled through the main axis center reduces mass and provides laser access to the tissue sample. Four tapped holes in the disk flange, spaced 90° apart on a 3" diameter circle, provide attachment points for the upper links. Tapped holes in the end opposite the flange and in the disk wall are used in attaching the disk arm and the Teflon® sleeve, respectively.

For final disk construction, a Teflon® liner 3.18-mm (0.125 inch) thick was bonded to the flange bottom using Loctite 454®. The liner was etched on the bonded side to facilitate bonding. A Teflon® sleeve of approximately 48.26-mm (1.9 inches) outer diameter (OD) was installed on the disk with screws. The assembled disk was then machine turned to specification by removing material from the liner face and the sleeve OD. Total finished drive disk mass is 145 grams.

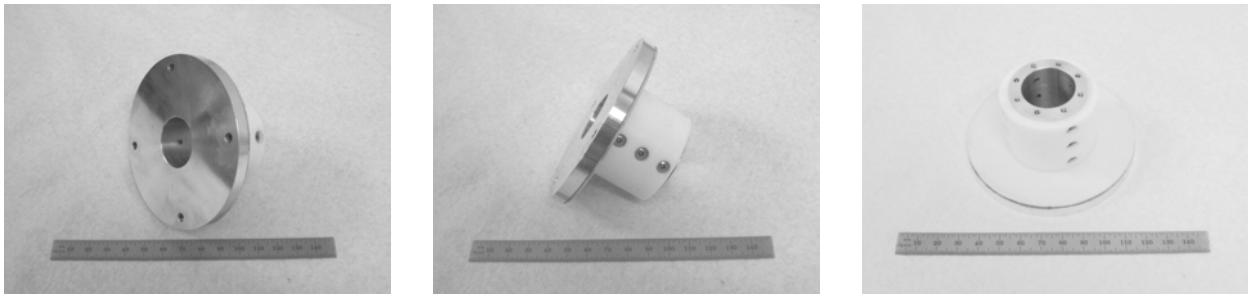

Fig. 5: Drive disk. From left to right: top, side, and bottom views.

Drive Arm

The drive arm attaches to the drive disk and transfers lower link motion to the drive disk. The arm has an OD of 69.34 mm (2.73 inches) and incorporates a low-friction Teflon® liner in its design (Fig. 6). A 25.4-mm (1 inch) hole in the face reduces mass and provides laser access to the tissue sample. A hole in the arm's lobe provides a connection point for the lower link and corresponds to an upper link connection point. Additional holes about the arm's ID are used in attaching the arm to the drive disk.

For final arm construction, a Teflon® liner of 3.18 mm (0.125 inch) thick was bonded to the arm using the same procedure as for the drive disk. A portion of the liner was cut away to provide clearance for the lower link. The assembled arm was then machine turned to specification by removing material from the liner face. The finished drive arm mass is 32 grams.

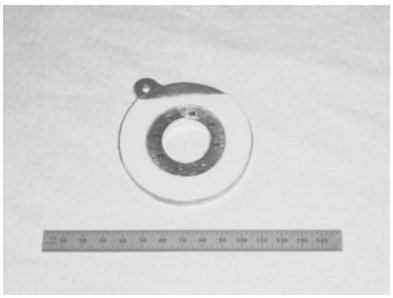

Fig. 6: Drive arm.

Links

The four upper links transfer the drive disk's rotary motion to the upper carriages. The lower link transfers the lower carriage's translational motion to the drive arm. Press-fit sleeve bearings of SAE 841 oil-impregnated sintered bronze are incorporated into the link design to ensure bind-free operation. All upper and lower link dimensions, including pivot point center-to-center distance, are identical. The links are 90.30 x 12.70 x 3.18 mm (3.555 x 0.500 x 0.125 inches), with a center-to-center distance of 77.58 mm (3.055 inches) between the pivot points (Fig. 7). The ID of the installed bearings is enlarged slightly from both ends using a tapered reamer to prevent potential binding. The upper links are a single piece design. The lower link is a two-piece, coupled design, one link being above the drive arm/lower carriage and the other below. The lower link pair is machined from titanium, selected for its excellent strength and weight characteristics.

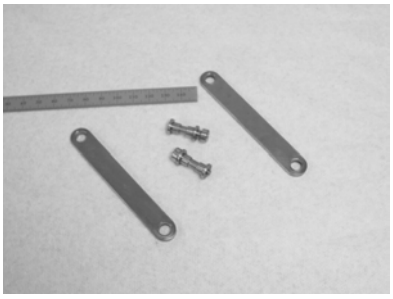

Fig. 7: Links (typical).

Carriages
The carriages (Fig. 8) are the moving platforms to which the tissue clamps attach. Frelon®-lined open bearings at the carriage corners ensure bind-free carriage motion. The four upper carriages are dimensionally identical, measuring 69.85 x 54.61 x 14.73 mm (2.75 x 2.15 x 0.58 inches). Material removed from each carriage's center region provides clearance for the clamp assembly and significantly reduces weight. A 6.35-mm (0.25-inch) wide slot, 25.4 -mm (1 inch) long, in the front cross-member receives the threaded rod of the clamp assembly. A tapped hole in the cross-member center serves as an upper link attachment point. Total carriage weight with bearings is approximately 64 grams.

The lower carriage differs from the upper carriages only in its cross-member design. The cross-member runs the length of the carriage and is centered with the main bores' primary axes. The main bores accept the bearings that ride on the liner shafts, or rails. Two holes, centered between the main bores and perpendicular to the bore axes, are machined through the cross-member. The hole in the cross-member front is used for link attachment and the hole at the back is used for rope attachment.

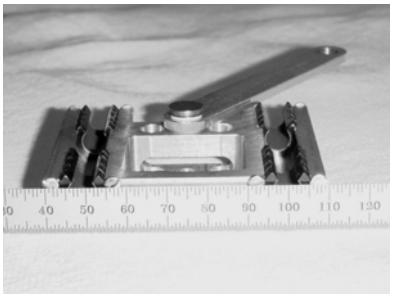

Fig. 8: Upper carriage.

Tissue Clamps
The tissue clamps are used to grip the tissue ends. Two things were considered to be of primary importance in the clamp design. The clamps need to be of minimal mass and should grip the tissue securely without cutting. The first design characteristic is desirable in that it minimizes the inertial effect of the clamp mass on the drive mechanism and the load data. The two-piece clamps (Fig. 9) weigh less than sixteen grams. The second characteristic is important because tissue slip or tearing at the clamp jaw would contaminate the test results. The cylindrical teeth installed on each jaw are knurled on their gripping face to enhance gripping action and are arranged in alternating opposition in the assembled clamp to prevent tissue slip and preserve tissue integrity.

The teeth in the upper and lower jaws are made from 3.18-mm (0.125 inch) round bar stock. Two tapped holes in each tooth, opposite the gripping face, provide a means of attaching the tooth to its corresponding jaw. The lower jaw has a single tooth and the upper jaw has a pair. In an assembled clamp, the tooth in the lower jaw is centered between the two teeth of the upper jaw, which are spaced 9.53 mm (0.375 inch) apart. Two 6.35-mm (0.24-inch) wide channels machined in the lower jaw's gripping face directly oppose the two teeth in the upper jaw. A similar, single channel in the upper jaw directly opposes the tooth in the lower jaw. This alternating arrangement of opposing teeth with corresponding channels clamps the tissue in a

wave-like pattern and eliminates tissue slip without compromising tissue integrity. Tapped holes at each end of the lower jaw, centered on the jaw midline, receive the screws used to attach the upper jaw. Mating holes are drilled at each end of the upper jaw.

In the upper jaw, four ball end-milled channels in the surface opposite the jaw face reduce weight, as do corner-rounding cuts at the jaw corners. The mass of the upper jaw, including attachment screws, is 7.3 grams. Similar channels and corner-rounding cuts in the lower jaw serve the same purpose. Lower jaw mass is 6.6 grams. The overall size of the each jaw is approximately 12.70 x 40.64 mm (0.5 x 1.6 inch), with a thickness of 9.53 mm (0.375 inch).

An internally threaded boss on the lower jaw threads onto one end of a sub-miniature load cell. The boss centerline is aligned with the tissue exit point from the clamp. An internally and externally threaded rod is attached to the load cell's opposite end. The rod's inner threads accept a threaded stud on the load cell. The rod's outer threads allow fore/aft positioning of the clamps when installed in the carriages. The entire assembly is attached to an upper carriage by placing the open end of the rod into the front cross-member slot and locking it in place with Nylon® nuts.

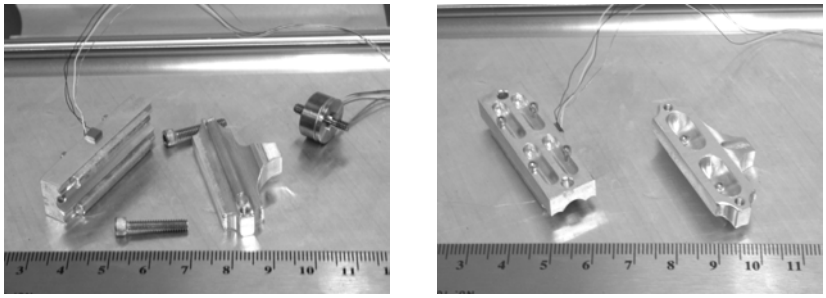

Fig. 9: Tissue clamp, inner and outer aspects.

Complete Assembly

The main bearing was placed in the main plate's center bore and secured with screws inserted from the plate bottom (Fig. 10). The drive disk was then placed in the main bearing, flange side up.

The lower link pieces were then attached to the drive arm pivot point. A single precision shoulder screw and two modified precision shoulder screws were used for this purpose. To ensure bind-free action at the pivot point, the two link ends corresponding to the drive arm were captured between two precision Teflon® washers. Precision stainless steel shims, placed against the Teflon® washers, allow each link end to be centered and aligned on its respective pivot. The shims also provide a means of optimizing link endplay. With the lower link pieces connected to the drive arm, the arm was then connected to the disk. The arm's lobe must be oriented directly beneath one of the threaded holes in the disk flange and liner side should contact the disk. The disk/arm unit should rotate freely in the bearing without play.

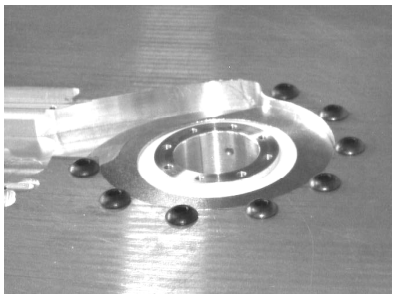

Fig. 10: Installed main bearing.

The lower carriage was placed on its shaft pair and connected to the link ends opposite the arm. The resulting arrangement places the drive arm centerline in the same plane as the carriage bearing centerline. The lower carriage should move freely with the disk when the assembly is rotated.

The upper links were attached to the bottom of their respective carriages and to the drive disk. Modified precision shoulder screws were used for this purpose. Washers and shims, identical to those described previously, were used on the upper links. They allow each link end to be centered and aligned horizontally with its pivot. The links were first attached to carriages. The carriages were then placed on the appropriate shaft pair, and the open link ends were connected to the drive disk (Fig. 11). The upper carriages should move freely when the drive disk is rotated. Attachment of each clamp assembly to the carriages was the final step in the assembly process.

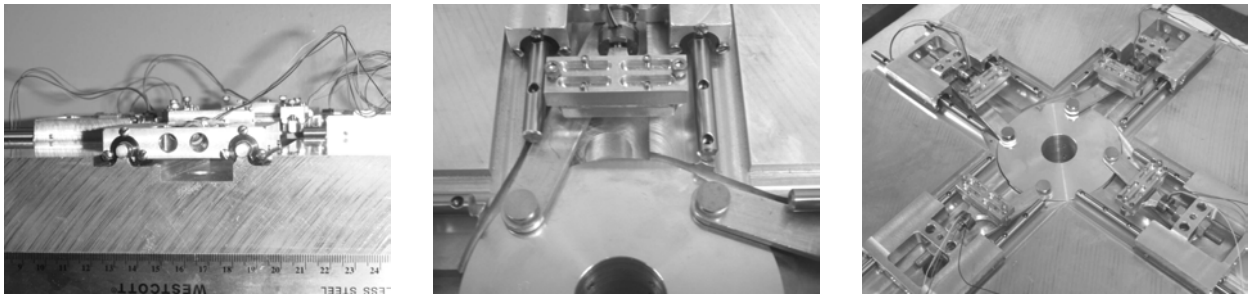

Fig. 11: Upper assembly. From left to right: carriage (end view), carriage (frontal view), entire assembly (top view).

DISCUSSION

A new device has been designed and fabricated for high-strain, high-speed biaxial tissue testing. The clamping mechanism has been shown to function up to 10 m/s in a high-speed Instron® machine using human cadaver aorta specimens. In addition to the development of the testing apparatus, protocols associated with its use have been developed also. The following is a brief treatment of basic specimen preparation and testing, and general device considerations.

Specimen Preparation Considerations

Specimens are dissected from human cadaver descending aortas (Fig. 12). A CNC machined die is used for this purpose. A specimen must not include regions where branching vessels exit the main trunk. With this in mind, the aorta segment is opened with a scalpel by making an

appropriate cut along its main axis. A sample is cut from the selected region of the aorta with the die oriented at an angle of 22.5º with respect to the long axis of the aorta. The die produces a sample with four arms that extend out perpendicular to a 10-mm square center. The base circle of each arm's edge is tangent to the square at its centerlines.

An array of sixteen dots is placed within the sample's center region with permanent marking ink. The array's column and row spacing is 2mm and it is framed by a 2mm border. Each arm is also marked on its centerline to facilitate accurate positioning in the test device. The four center dots are used in finding the stretch ratio and the twelve outer 12 dots assist in determining if there is any shear effect due to clamping or tissue shape. The entire array of dots is used as an aid in determining the sample's rupture pattern (angle of rupture, location, etc.)

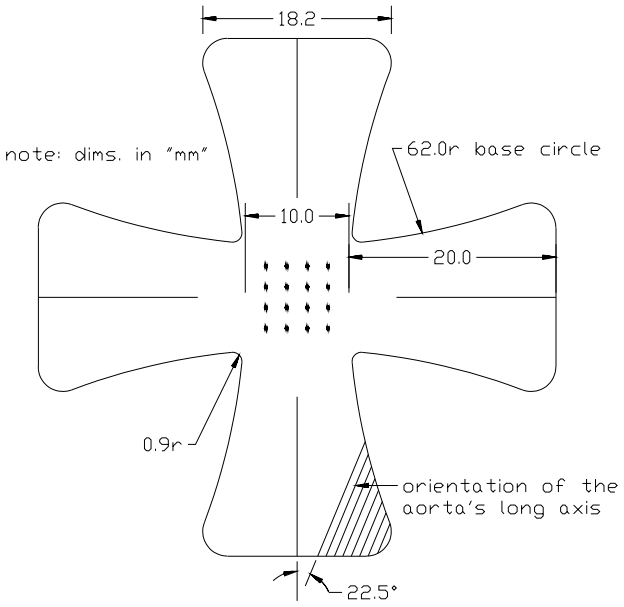

Fig. 12: Example tissue sample characteristics.

Specimen Testing Considerations
Each sample is kept in saline prior to testing, and is wetted with saline spray during testing. Each sample is placed in the test device with each of the four arms positioned over a clamp's lower jaw. The upper clamp jaws are then attached and tightened only to a point that facilitates positioning of the sample. The clamps are fully tightened when each arm's centerline aligns with the centerline of its respective clamp and each clamp is centered on the drive disk centerline.

Two lasers, focused on the top and bottom surfaces of the tissue sample, measure sample thickness throughout a given test. The laser beams are focused directly on the sample's center during a test. Measurements, made on the positioned sample prior to testing, are taken with the lasers at various points within the sample's center square (marked by dots). The recorded values are used to calculate the sample's average thickness and aid in determining the change in

thickness as well as the true/engineering stresses along each direction. A camera mounted above the sample is used to record each test at 1000 fps.

A retracting pneumatic cylinder (Fig. 13) attached to the lower carriage produces motion in the test device. Compressed air released to the cylinder by means of a solenoid valve drives the cylinder. Initial slack in the low-stretch, high-strength Technora® rope (6.9 kN work load limit) that connects the cylinder to the lower carriage allows the cylinder to achieve the desired test speed before initiating motion in the lower carriage. Speed is modulated by air pressure and backpressure valves. Drive disk/drive arm unit rotation, induced by lower carriage motion, produces identical upper carriage motion in four directions away from the disk center. Each carriage moves outward from the disk center approximately 51 mm, with each clamp initially being at a point approximately 32 mm from the disk center, as measured from the clamp edge nearest the center. A second solenoid valve on the cylinder's exhaust port, initially open, is closed in combination with the intake solenoid to brake cylinder motion. Wedge-shaped polyurethane dampers engage the upper links at the extreme end of the drive disk's rotation to prevent over-travel and damage to the device.

The sub-miniature Entran® load cells (Model# ELFM-T2E-100L) mounted behind the clamps record the load at their respective arm. The 450-N capacity load cells weigh approximately 5 grams. A miniature accelerometer mounted on each clamp allows for mass correction of the load.

The strain/stretch ratio for each axis is calculated using the video data and the formula below.

$$\lambda_1(t) = \frac{l_{x1}(t)}{l_{x1}^0} = \frac{\text{Average Distance between two central dots along X}}{\text{Original Distance between two central dots along X (2 mm)}}$$

Force-elongation, true stress-extension ratio, or engineering stress-strain are plotted for both directions using compensated load values.

General Considerations

Sacks (2001) reviewed the importance of tissue sample geometry and boundary conditions. Waldman et al. (1999) noted the different stress and strain field in the vicinity of attachments to the tissue, but stated that within the typical marker field, far from the attachments, fiber reorientation was a function of local tissue strains and had little to do with the method of attachment.

This result cannot be reconciled completely with the later findings of Waldman and Lee (2002), resulting from the examination of the relative effects of tethering and clamping as methods of tissue attachment. Different stress-strain responses were demonstrated depending on the attachment method. It was suggested that neither method was ideal, and that each would influence the results in some way. Tissue tethering generates point loads, which create dramatic local fiber reorientation and discrete loading effects, including tissue tearing. Further, the tethering approach produces a softer stress-strain response. Tissue clamping improves mechanical coupling and therefore stress transfer. The clamping approach produces a stiffer stress-strain response. It is unclear the degree of coupling that can be achieved using tethers, especially in tests that use electromechanical vibrators (e.g. Bass et al., 2001).

In addition to examining the effect of boundary conditions, Waldman and Lee (2002) discussed the effect of specimen geometry. Typical specimen geometries are either square or cruciate shapes. For cruciate specimens, it was found that shorter arms reduced extensibility and produced stiffer results. Shorter arms also reduced shearing and rigid-body rotation of the specimen.

Tissue tethering will not work well for high load, extension, and rate applications. Properly designed tissue clamps and appropriately sized and oriented cruciate tissue specimens can be combined to produce reasonable geometry and boundary conditions for the determination of tissue properties at rates commensurate with automotive-injury. These properties can be used to develop better constitutive descriptions of the behavior of the aorta for application in finite element models such as that of Shah et al. (2001). Further, better understanding of the behavior of the aorta at the tissue level will aid in the understanding of traumatic rupture of the aorta in general.

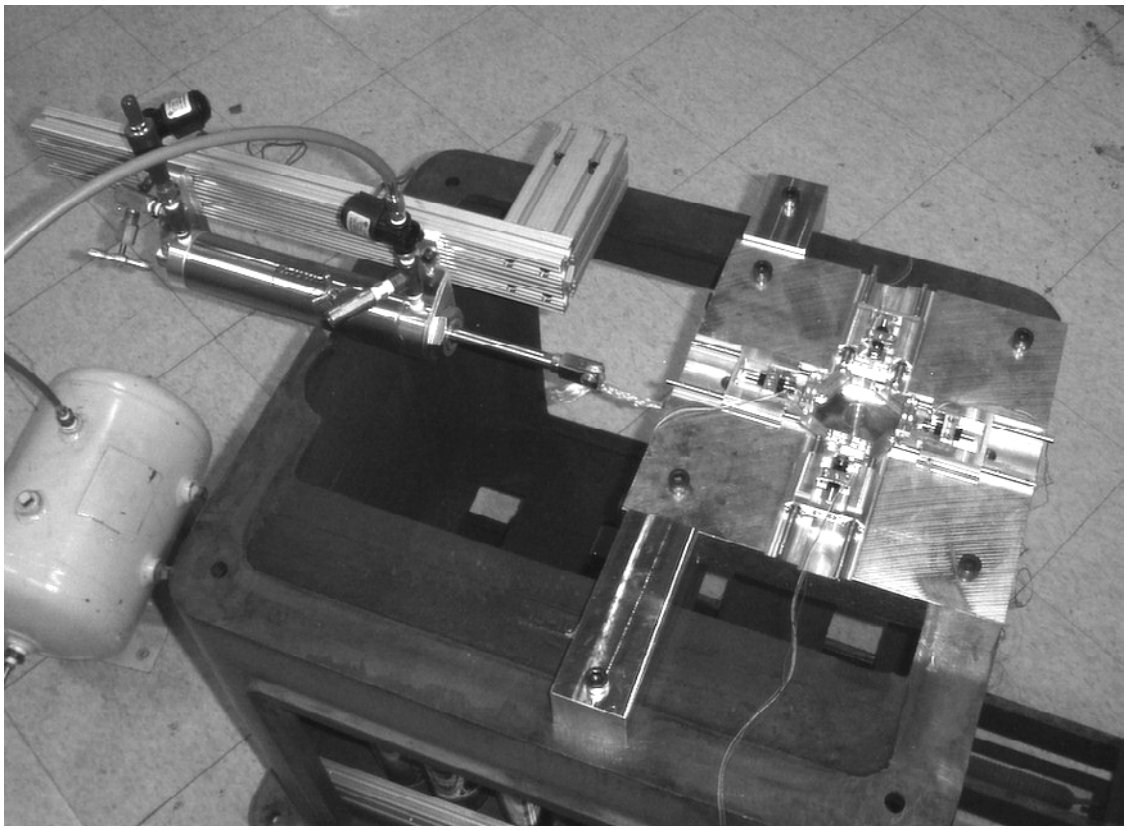

Fig. 13: The pneumatic drive mechanism attached to the tissue testing apparatus, mounted to a machine base.

ACKNOWLEDGMENT
This study is funded by The George Washington University.

REFERENCES

Bass, CR; Darvish, K; Bush, B, Crandall, JR; Srinivasan, SCM; Tribble, C; Fiser, S; Tourret, L; Evans, JC; Patrie, J; Wang, C (2001) Material properties for modeling traumatic aortic rupture. Stapp Car Crash Journal, 45:143-160.

Bergel, D.H (1961). The static elastic properties of the arterial wall. *J Physiol-London*, 156:445-457.

Boreik, AM; Kelly, NG; Rodarte, JR; Wilson, TA (2000) Biaxial constitutive relations for the passive canine diaphragm. *J Appl Physiol*, 89:2187-2190.

Collins, R., and Hu, WCL (1972) Dynamic deformation experiments on aortic tissue. *J Biomech*, 5:333-335.

Demer, LL; and Yin, FCP (1983) Passive biaxial mechanical properties of isolated canine myocardium." *J Physiol*, 339:615-630.

Fung, YC (1993) Biomechanics: Mechanical properties of living tissues. Springer-Verlag, New York, NY.

Gow, BS; and Taylor, MG (1968) Measurement of viscoelastic properties of arteries in living dogs. *Circ Res*, 23:111-122.

Hallock, P and Benson, IC (1937) Studies on the elastic properties of human isolated aorta. *J Clin Invest* 16:595.

Lundevall, J (1964) The mechanism of traumatic rupture of the aorta. *Acta Path Mic Sc*, 62: 34-46.

Mohan, D and Melvin, JW (1982) Failure properties of passive human aortic tissue. I - uniaxial tension tests. *J Biomech*, 15:887-902.

Mohan, D and Melvin, JW (1983) Failure properties of passive human aortic tissue. II - biaxial tension tests. *J Biomech*, 16:31-44.

Nielsen, PMF; Hunter, PJ; Smaill, BH (1991) Biaxial testing of membrane biomaterials: testing equipment and procedures. *J Biomech Eng-T ASME*, 113:295-300.

Sacks, MS and Chuong, CJ (1993) Biaxial mechanical properties of passive right ventricular free wall myocardium. *J Biomech Eng-T ASME*, 115:202-205.

Sacks, MS (2001) Biaxial mechanical evaluation of planar biological materials. *J Elasticity*, 61:199-246.

Shah, CS; Yang, KH; Hardy, WN; Wang, HK; King, AI (2001) Development of a computer model to predict aortic rupture due to impact loading. *Stapp Car Crash Journal*, 45:161-182.

Silver, FH; Chistiansen, DL; Buntin, CM (1989) Mechanical properties of the aorta: A review. *Crit Rev Biomed Eng*, 17(4):323-358.

Viano, DC (1983) Biomechanics of non-penetrating Aortic Trauma: A review. *Proc. 27th Stapp Car Crash Conference*, pp.109-114, SAE Paper No.831608.

Waldman, SD; Lee, MJ (2002) Boundary conditions during biaxial testing of planar connective tissues. Part 1: Dynamic Behavior. *J Mater Sci Mater Med*, 13(10):933-938.

Waldman, SD; Sacks, MS; Lee, MJ (1999) Imposed state of deformation determines local collagen fibre orientation but not apparent mechanical properties. *Biomed Sci Instrum*, 35:51-56.

Zhou, J and Fung, YC (1997). The degree of nonlinearity and anisotropy of blood vessel elasticity. *P Natl Acad Sci USA*, 94:14255-14260.

Drawing 21: TISSUE CLAMP (upper jaw)

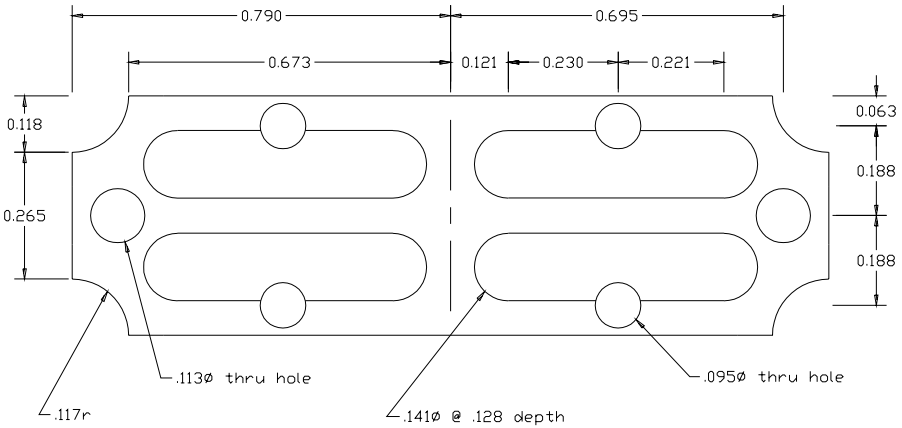

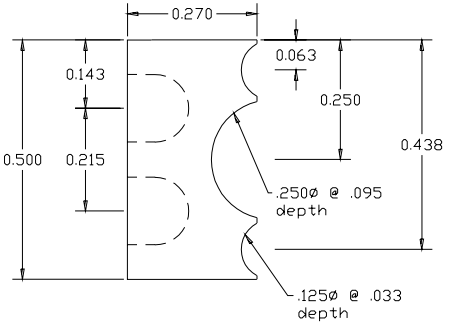

note: all dims in inches and
some lines not shown

Material: 6061-T6 aluminum

Quantity: 4

Drawing 22: TISSUE CLAMP (lower jaw)

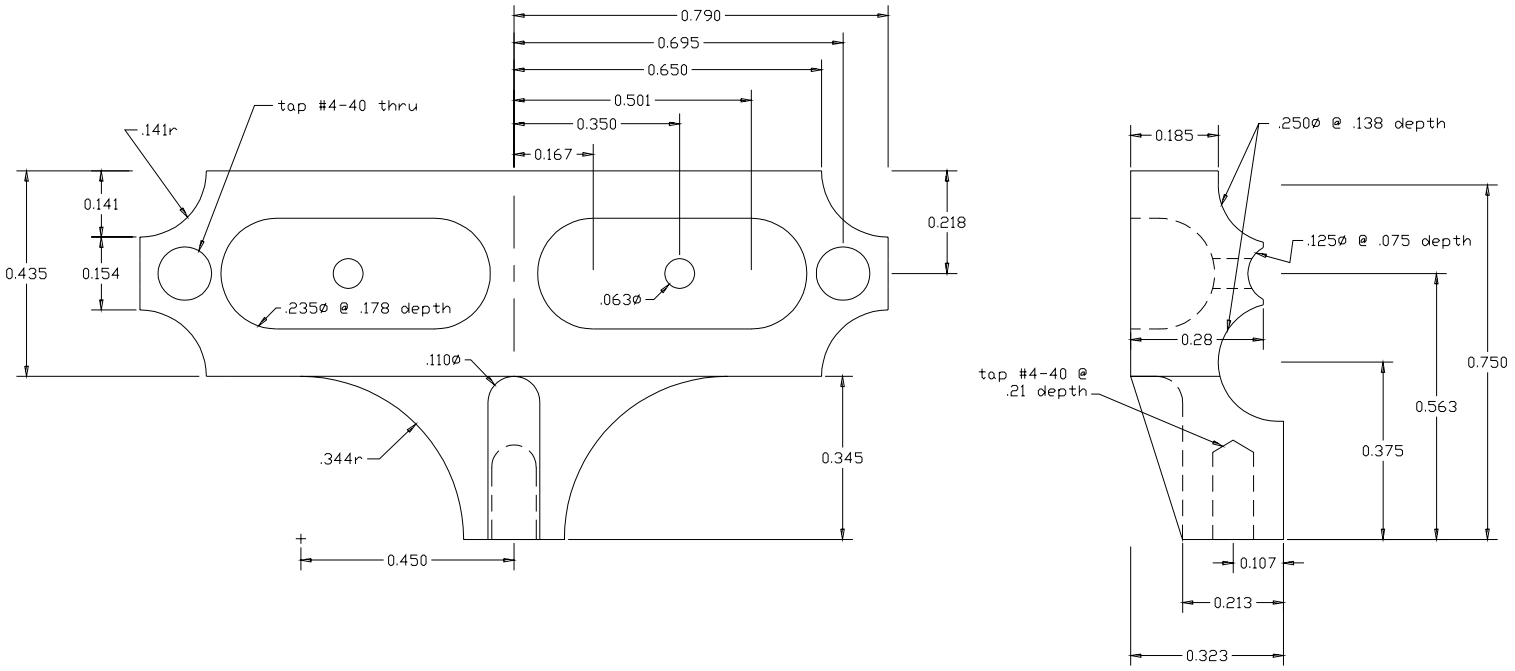

note: all dims in inches and
some lines not shown

Material: 6061-T6 aluminum

Quantity: 4

Drawing 23: CLAMP TOOTH

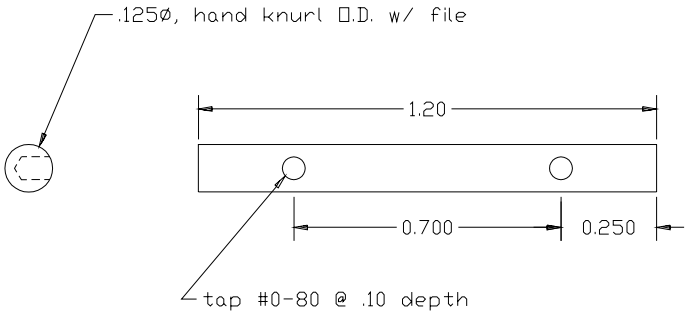

note: all dims in inches

Material: 6061-T6 aluminum

Quantity: 12

Drawing 25: CARRIAGE (upper)

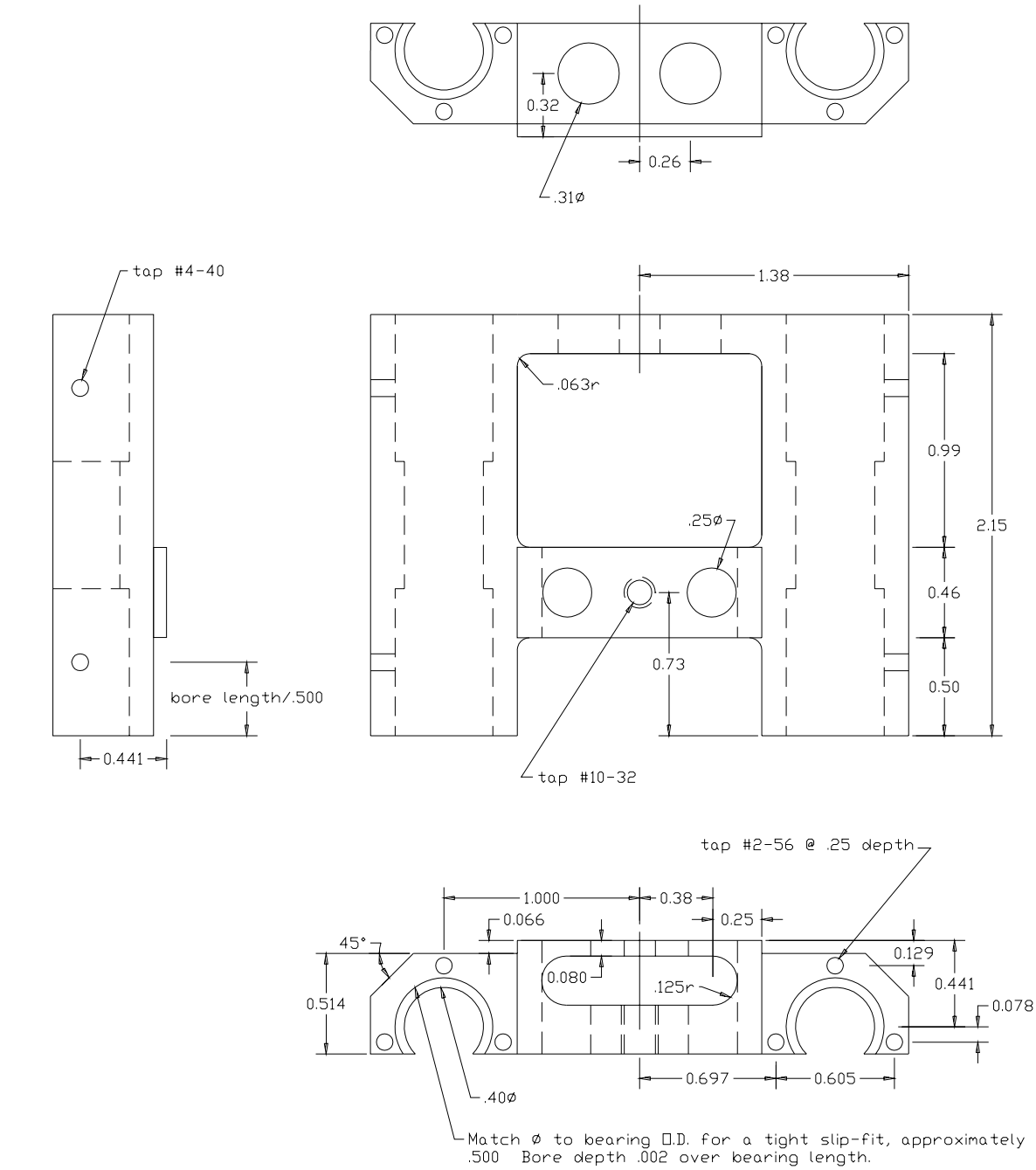

note: all dims in inches and some lines not shown

Material: 6061-T6 aluminum

Quantity: 4